Fast reconnection in high-Lundquist-number plasmas due to the plasmoid Instability

Cite as: Phys. Plasmas **16**, 112102 (2009); https://doi.org/10.1063/1.3264103
Submitted: 01 July 2009 . Accepted: 26 October 2009 . Published Online: 11 November 2009

A. Bhattacharjee, Yi-Min Huang, H. Yang, and B. Rogers

Fast reconnection in high-Lundquist-number plasmas due to the plasmoid Instability

A. Bhattacharjee,[1] Yi-Min Huang,[1] H. Yang,[2] and B. Rogers[2]
[1]*Center for Integrated Computation and Analysis of Reconnection and Turbulence, University of New Hampshire, Durham, New Hampshire 03824, USA*
[2]*Center for Integrated Computation and Analysis of Reconnection and Turbulence, Dartmouth College, Hanover, New Hampshire 03825, USA*

(Received 1 July 2009; accepted 26 October 2009; published online 11 November 2009)

Thin current sheets in systems of large size that exceed a critical value of the Lundquist number are unstable to a super-Alfvénic tearing instability, referred to hereafter as the plasmoid instability. The scaling of the growth rate of the most rapidly growing plasmoid instability with respect to the Lundquist number is shown to follow from the classical dispersion relation for tearing modes. As a result of this instability, the system realizes a nonlinear reconnection rate that appears to be weakly dependent on the Lundquist number, and larger than the Sweet–Parker rate by nearly an order of magnitude (for the range of Lundquist numbers considered). This regime of fast reconnection is realizable in a dynamic and highly unstable thin current sheet, without requiring the current sheet to be turbulent. © *2009 American Institute of Physics*. [doi:10.1063/1.3264103]

I. INTRODUCTION

The problem of fast reconnection in high-Lundquist-number plasmas has attracted a great deal of attention since the inception of the classical Sweet–Parker[1,2] and Petschek[3] models. In the Sweet–Parker model, the reconnection layer has the structure of *Y*-points, with a length of the order of the system size L and a width given by $\delta_{SP}=L/S_L^{1/2}$, where S_L is the Lundquist number based on the system size. The steady-state reconnection time scale τ_{SP} is a strong function of S_L, and increases as $S_L^{1/2}$. For weakly collisional systems such as the solar corona, the Lundquist number is typically very large ($\sim 10^{12}-10^{14}$) and hence, the time scale τ_{SP} is of the order of years, which is much too long to account for fast events such as solar flares. A similar difficulty appears when the Sweet–Parker model (equivalently, the Kadomtsev model[4]) is applied to the problem of sawtooth crashes in high-temperature tokamaks, where the predictions of the model for the sawtooth crash time is significantly larger than that observed. These inadequacies of the Sweet–Parker model have led to the point of view that within the framework of resistive magnetohydrodynamics (MHD), it is not possible to realize fast reconnection for high-S plasmas.

In this paper, we demonstrate that this widely accepted point of view is not correct for large systems, characterized by high Lundquist number ($S_L \geq 3\times 10^4$). By large systems, we mean systems for which the aspect ratio of the thin current sheet δ_{SP}/L is much smaller than unity. In such systems, over a critical value of S_L, there appears to be three qualitatively distinct phases during the nonlinear evolution of reconnection. In the early nonlinear regime, the system evolves to a quasisteady but transient state with the characteristics of Sweet–Parker reconnection—an extended thin current sheet in which reconnection occurs on the time scale τ_{SP}. This quasisteady regime is short-lived, and is followed by a second phase in which a rapid secondary instability (referred to hereafter as the plasmoid instability) occurs and produces plasmoids copiously. Although the presence of this instability has been recognized for some time,[5–10] it is only relatively recently that the precise scaling properties of the most rapidly growing plasmoid instability have been established.[11–13] We demonstrate here that the key properties of this instability can be obtained as a simple extension of the classical dispersion relation of tearing modes,[14] applied to a Sweet–Parker current layer of width δ_{SP}. The instability is followed by a third nonlinear phase in which the system exhibits rapid and impulsive reconnection mediated by a hierarchy of current sheets[9] with widths that are much smaller than δ_{SP} with a Lundquist number dependency that decays faster than $S_L^{-1/2}$. When averaged over time, reconnection in the third nonlinear regime proceeds at a rate much faster than Sweet–Parker. Unlike the Sweet–Parker reconnection rate, which decays as $S_L^{-1/2}$ with increasing S_L, the reconnection rate in the third nonlinear phase appears to have a weak dependence on S_L.

II. LINEAR PLASMOID INSTABILITY

To fix ideas, consider a Harris sheet of width a with the equilibrium magnetic field $\mathbf{B}=B_0\tanh(z/a)\hat{\mathbf{x}}$, which reverses sign at the $z=0$ surface. According to classical linear tearing instability theory, the tearing mode growth rate for the constant-ψ and nonconstant-ψ modes are as follows, respectively,[14]

$$\gamma\tau_A \sim \begin{cases} S^{-3/5}(ka)^{-2/5}(1-k^2a^2)^{2/5}, & kaS^{1/4} \gg 1, \\ S^{-1/3}(ka)^{2/3}, & kaS^{1/4} \ll 1, \quad ka \ll 1. \end{cases} \tag{1}$$

Here $S=\tau_R/\tau_A$, where $\tau_A=a/v_A=a(4\pi\rho)^{1/2}/B_0$ is the Alfvén time, $\tau_R=4\pi a^2/(\eta c^2)$ is the resistive diffusion time, ρ is the mass density, η is the resistivity of the plasma, assumed to be a constant, and c is the speed of light. We note that the Lundquist number S_L, introduced earlier, is related to S

through the relation, $S_L=S/\varepsilon$, where $\varepsilon=a/L$. According to the dispersion relation (1), the transition from constant-ψ to nonconstant-ψ modes occurs at $kaS^{1/4}\sim 1$, with a peak growth rate that scales as $\gamma_{\max}\tau_A\sim S^{-1/2}$. Since both branches of the tearing mode dispersion relation (1) yield instabilities that grow at a rate proportional to S raised to a fractional *negative* exponent, it may seem surprising upon first glance that there exists a super-Alfvénic tearing instability that actually grows at a rate proportional to S_L raised to a fractional *positive* exponent. The key point is that unlike the Harris sheet, which is characterized by an equilibrium width a, which is independent of the resistivity, the Sweet–Parker current sheet is characterized by a width $\delta_{\rm SP}$, which has a strong dependence on the resistivity. To connect with the results obtained in Ref. 11, we introduce the dimensionless wave number $\kappa=kL=ka/\varepsilon$, and the dimensionless growth rate $\gamma_L=\gamma\tau_A/\varepsilon$. In terms of dimensionless parameters κ, ε, and S_L, the maximum growth rate is given by $\gamma_{L,\max}\sim\varepsilon^{-2/3}\kappa^{2/3}S_L^{-1/3}$, and it occurs at the wave number $\kappa_{\max}\sim\varepsilon^{-5/4}S_L^{-1/4}$. For a Sweet–Parker current sheet, which obeys $\varepsilon\sim S_L^{-1/2}$, we then obtain $\kappa_{\max}\sim S_L^{3/8}$, and the maximum growth rate $\gamma_{L,\max}\sim S_L^{1/4}$. Note that the number of plasmoids generated in the linear regime of this instability scales as $\kappa_{\max}$. These scaling relations are completely consistent with the results obtained for the fastest growing instability in Ref. 11.

The rapidity of the plasmoid instability is not limited to Sweet–Parker current sheets, for we can easily extend the results obtained above to current sheets that may be narrower than Sweet–Parker current sheets (for the same value of S_L). If we write $\varepsilon\sim S_L^{-\alpha}$, where $\alpha>0$, we obtain $\kappa_{\max}\sim S_L^{(5\alpha-1)/4}$ and $\gamma_{L,\max}\sim S_L^{(3\alpha-1)/2}$. It follows then that in sheets for which $\alpha>1/2$, the plasmoid instability will grow even more rapidly than in Sweet–Parker current sheets of the same Lundquist number (for which $\alpha=1/2$).

III. NONLINEAR EVOLUTION

Our nonlinear study is carried in two-dimensional (2D), doubly periodic geometry using fully compressible MHD equations (in dimensionless form). The magnetic field is represented as $\mathbf{B}=\nabla\psi(x,z)\times\hat{\mathbf{y}}$ where ψ is a flux function and y is the ignorable coordinate, $\mathbf{v}=(v_x,v_z)$ is the fluid velocity, and p is the scalar pressure, assumed to obey an isothermal equation of state, $p=2\rho T$, where ρ is the density and T is a constant temperature. The relevant dynamical equations are

$$\partial_t\rho+\nabla\cdot(\rho\mathbf{v})=0, \tag{2}$$

$$\partial_t(\rho\mathbf{v})+\nabla\cdot(\rho\mathbf{v}\mathbf{v})=-\nabla p-\nabla\psi\nabla^2\psi, \tag{3}$$

$$\partial_t\psi+\mathbf{v}\cdot\nabla\psi=\eta\nabla^2\psi. \tag{4}$$

Our numerical algorithm[15] approximates spatial derivatives by finite differences with a five-point stencil in each direction, and time derivatives by a second-order accurate trapezoidal leapfrog method. We use variable grids in order to resolve the sharp spatial gradients in the reconnection layer. The initial condition consists of four flux tubes, which exhibit the coalescence instability. The initial equilibrium state is given by $\psi=A_0\sin(2\pi x/L)\sin(2\pi z/L)$. In the results that follow, we take $L=\sqrt{2}$ and $A_0=L/\sqrt{2}\pi$, which produces a peak magnetic field of unit magnitude in equilibrium. The initial density is taken to be approximately unity and the pressure (calculated from the isothermal equation of state with $T=3$ for all simulations) is approximately equal to 6. Both density and pressure profiles are assumed to have a weak spatial dependence in order to satisfy the magnetostatic equilibrium condition.

The flux tubes in equilibrium are unstable to the coalescence instability, and produce an extended current sheet nonlinearly. Figure 1 shows a time-sequence of the current density $J_y(x,z)$ for $S_L=6.28\times10^5$, which exhibits the three stages of the nonlinear dynamics, discussed above. (Here time is measured in units of $\tau_{\rm AL}=L/V_A$.) For convenience of visualization, we have rotated the current sheet by 45° to make it horizontal. Frame (a) represents the first phase, the so-called Sweet–Parker phase of the instability, which is characterized by the formation of extended, system-size current sheets with the structure of Y-points. Subsequently, this current sheet becomes spontaneously unstable to the plasmoid instability, producing the second phase of nonlinear evolution [frame (b)]. This second phase is followed by a third phase in which reconnection is typically impulsive (or bursty), significantly faster than Sweet–Parker, and associated with the spontaneous development and ejection of plasmoids in the outflow direction(s) [frame (c)]. As mentioned above, the third phase has multiple stages. As the secondary instability develops, the initial Sweet–Parker current sheet breaks up, producing islands that separate shorter, narrower and more intense current sheets of width $\delta<\delta_{\rm SP}$. These intermediate current sheets become unstable to secondary tearing instabilities of higher growth rate than those of the initial Sweet–Parker sheet, and lead to a regime of faster reconnection [frame (d)].

In Fig. 2, we show the time-history of the (normalized) reconnection rate, multiplied by $S_L^{1/2}$, for three simulations, including the high-S simulation (black plot) shown in Fig. 1. The reconnection layer is along the x direction. We use a uniform grid along x. The grid along z is highly packed around $z=0$. Table I summarizes the number of grid points as well as (the smallest) grid size in each direction. (The Sweet–Parker thickness is included for reference.) The reconnection rate is calculated by taking the time derivative of the maximum stream function in the reconnection layer, normalized to the product of the upstream magnetic field and the Alfvén speed, and smoothed over $0.4\tau_{\rm AL}$ to eliminate rapid variations in a very dynamic current sheet. In Fig. 2, the black curve corresponds to $S_L=6.28\times10^5$, and describes the time-evolution of the equilibrium which is initially unstable to the coalescence instability and produces a Sweet–Parker current sheet that persists until about $t\sim3$. After this point in time, the plasmoid instability develops, breaking up the long Sweet–Parker current sheet. (While the qualitative features of the instability are those of the linear plasmoid instability discussed above, it is difficult to test the precise scaling properties of the linear instability during a nonlinear evolution.) There is a rapid enhancement in the reconnection rate that remains impulsive and fluctuates widely even as the rate

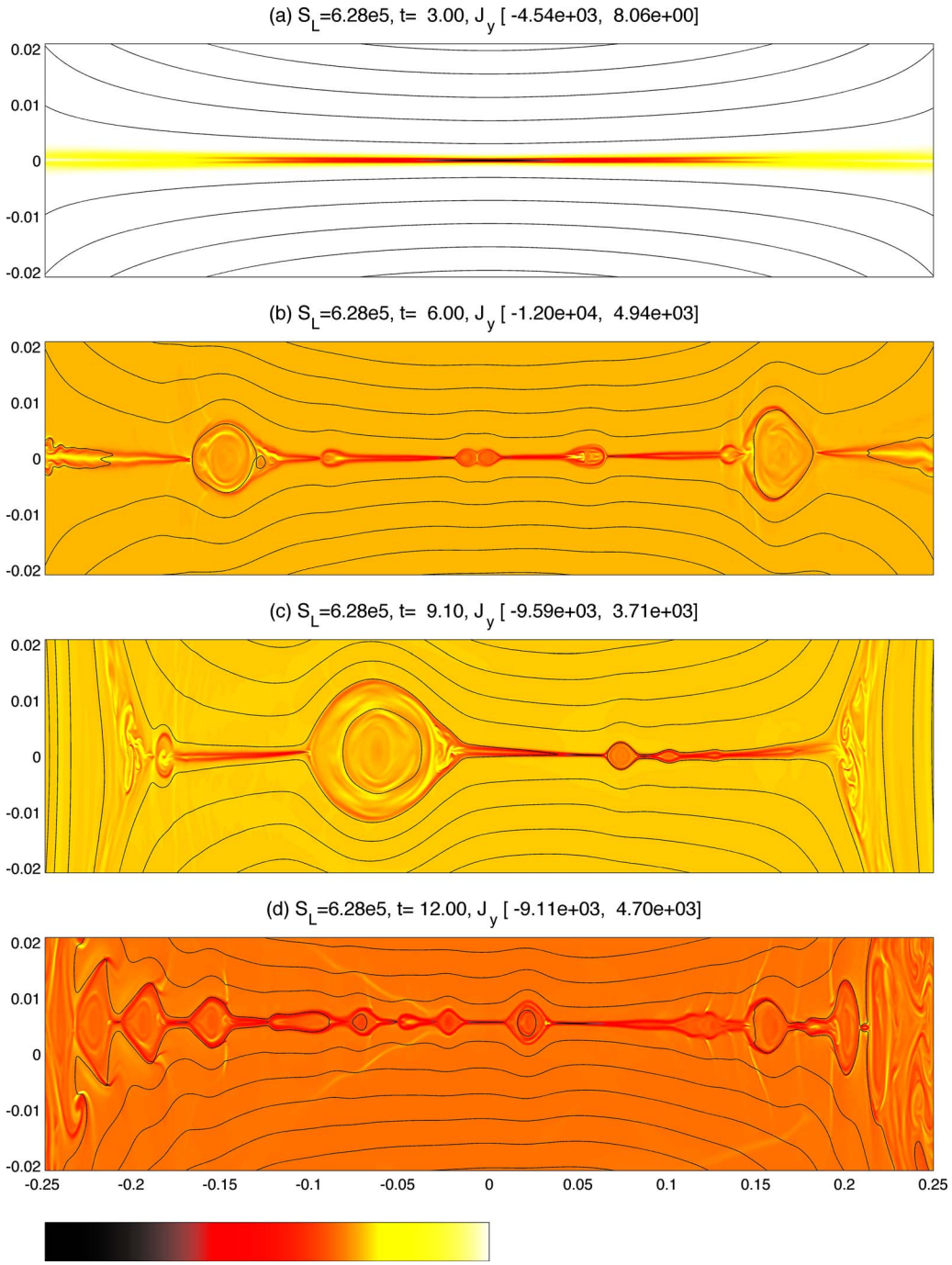

FIG. 1. (Color online) Time-sequence of the nonlinear evolution of the current density J_y of a Sweet–Parker current sheet in a large system of Lundquist number $S_L=6.28\times10^5$. The black lines represent surfaces of constant ψ.

tends to settles down to a plateau, until about $t\sim9$. At this stage of the third nonlinear phase, some of the small islands produced by the secondary instability coalesce to form larger islands that are convected toward the boundaries. (If the islands grow to large size but are constrained to stay fixed at the center of the computational domain by reason of symmetries imposed in the simulations, the third nonlinear phase may be short-lived, and the reconnection rate may fall rapidly.) At about this point in time, the extended current sheet shows yet another burst of secondary tearing activity producing multiple plasmoids, and a consequent enhancement in the reconnection rate, which at about $t\sim12$ attains nearly an order of magnitude higher than the Sweet–Parker rate at this value of S_L. Due to insufficient spatial resolution, caused by the slow drift of the current sheet away from the region where the grid points along z are clustered, we are not able to carry these simulations forward longer in time.

The plasmoid instability of Sweet–Parker sheets occurs after S_L exceeds a critical value, determined numerically to be approximately 3×10^4 in the present study. Like the black curve, the blue dashed curve in Fig. 2 corresponds to another value of S_L $(=2.51\times10^5)$ above the threshold and shows generically similar behavior, while the red dashed curve corresponds to a value $(=3.14\times10^4)$ at about the threshold. We

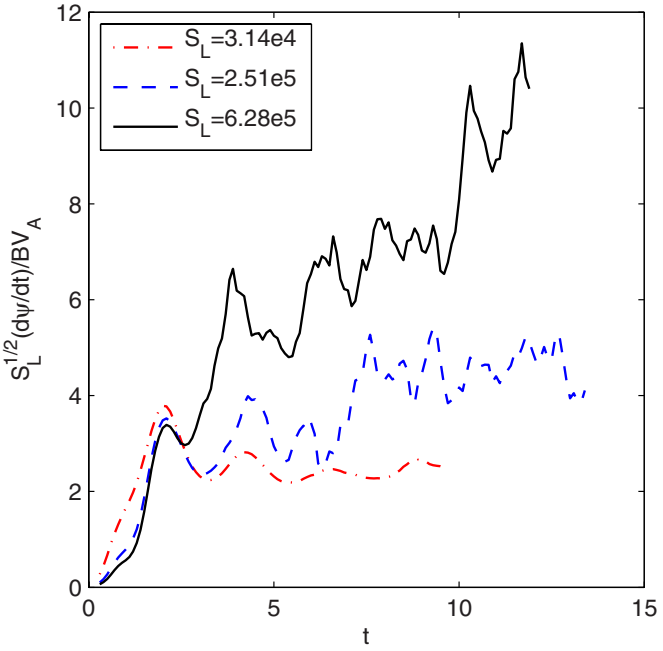

FIG. 2. (Color online) Time-evolution of the scaled reconnection rate for three values of the Lundquist number. The black curve corresponds to the case shown in Fig. 1.

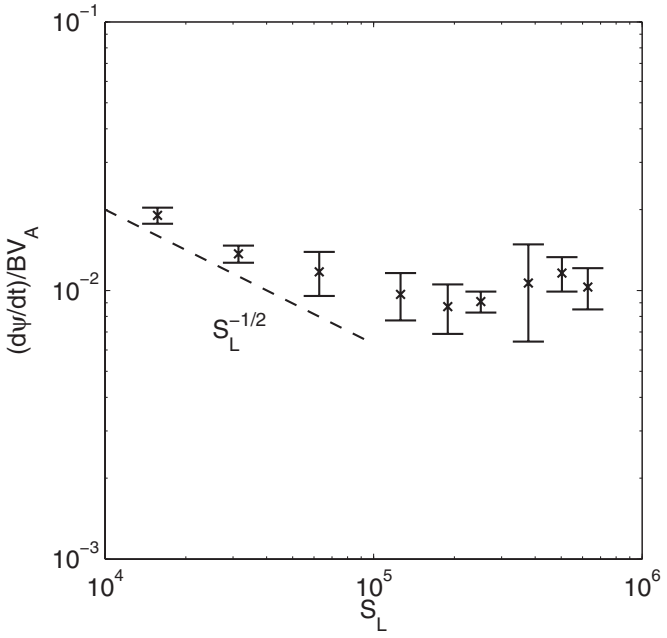

FIG. 3. Averaged reconnection rate as a function of S_L. Below $S_L \approx 3 \times 10^4$, the reconnection rate is Sweet–Parker and decays as $S_L^{-1/2}$, shown by the dotted line. Above this threshold, the reconnection rate becomes weakly dependent on S_L.

have identified the plateau regions in these curves by inspection, and stated the corresponding time intervals in Table I. There is clearly an element of arbitrariness in this identification, because the underlying dynamics is not quasisteady. In fact, the dynamics is generically impulsive, strongly time-dependent, involving the growth and ejection of multiple plasmoids, and complicated by the sloshing of coalescing islands as well as the tilt and slow drift of the current sheet away from the central region. The sloshing is most clearly seen in the oscillations of the red curve, where the first peak corresponds to the highest reconnection rate, after which the system settles down to a Sweet–Parker-like plateau regime. A rough definition of the plateau region is when the reconnection rate appears to fluctuate about a relatively steady value. If the Lundquist number of the simulation is above the threshold for the plasmoid instability, the plateau region is typically characterized by the presence of multiple islands.

Figure 3 shows a plot of the averaged reconnection rate (normalized) as a function of S_L. The averaged reconnection rate is calculated by averaging the smoothed reconnection rate curve over the plateau region. The error bar is calculated from the standard deviation of the data points in the plateau region. Our simulations suggest that below a threshold, $S_L \approx 3 \times 10^4$, the reconnection rate exhibits Sweet–Parker scaling. Over this threshold, the averaged reconnection rate exhibits a much weaker dependency on S_L. At high values of S_L, the average reconnection rate exceeds the Sweet–Parker rate by nearly an order of magnitude.

Since reconnection in this system is inherently impulsive and nonsteady, the diagnostic used above to compute the average reconnection rate is subject to significant time-variability. Therefore, we present the results of another diagnostic that measures reconnection, and is complementary to the results shown in Fig. 3. For this diagnostic, we compute the time needed to reconnect a significant portion of the flux in the islands. We note that $\psi=0$ at the separatrix at $t=0$, and that the initial amount flux within each island is 0.318. We define a characteristic reconnection time as the time taken for the value of ψ at the separatrix to change from $\psi=0.02$ to $\psi=0.14$. (This change corresponds to approximately 40% of the initial flux.) We start the measurement at $\psi=0.02$ instead of $\psi=0$ to skip over the initial transients and allow the linear plasmoid instability to develop. The result is shown in Fig. 4, and is qualitatively similar to that seen in Fig. 3, that is, the time for reconnection decreases significantly from the prediction of the Sweet–Parker theory once we cross the thresh-

TABLE I. Details of the spatial resolution and the plateau regime for the runs shown in Fig. 2. We use variable grids. N_x and N_z are the number of grid points in the x and z directions, respectively.

S	Δx	Δz	N_x	N_z	$S_L^{-1/2}$	Plateau regime
3.14×10^4	6.7×10^{-4}	5×10^{-4}	1501	501	5.6×10^{-3}	2.9–8.9
2.51×10^5	5×10^{-4}	9.4×10^{-5}	2001	1001	2×10^{-3}	6.9–13.0
6.28×10^5	3.3×10^{-4}	3.9×10^{-5}	3001	1501	1.26×10^{-3}	6.9–11.6

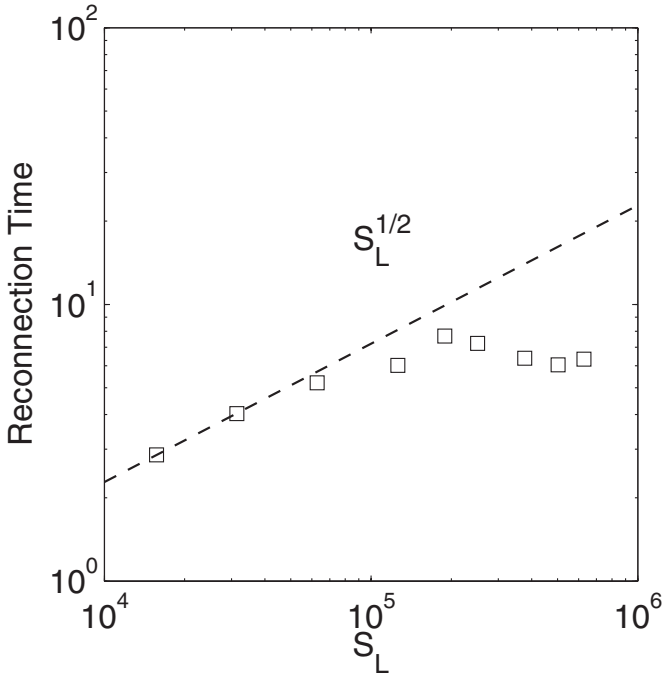

FIG. 4. Time to reconnect approximately 40% of the initial flux as a function of S_L. For details, see text. The dashed line indicates the prediction of Sweet–Parker theory.

old in Lundquist number for the onset of the plasmoid instability.

These results bear qualitative resemblance and are complementary to those reported in a concurrent study,[16] where 2D, fully electromagnetic particle-in-cell simulations that include a collision operator show a regime of fast reconnection brought about by the onset of secondary tearing instabilities. Since the physical models underlying the simulations presented here and in Ref. 16 are quite different, it is not surprising that there are some important differences between the two studies. The initial Sweet–Parker current sheet realized in Ref. 16 shows clear evidence of the plasmoid instability, and the width of subsequent intermediate current sheet segments becomes much narrower as time progresses, as in the present study. Whereas this narrowing is controlled entirely by the value of the Lundquist number and can continue without the intervention of kinetic effects in the present study, kinetic effects inevitably intervene in Ref. 16 when the current sheet becomes of the order of ion skin depth. For systems of moderate size (of the order of $200d_i$ or less), when $\delta \leq d_i$, the simulations in Ref. 16 show the onset of fast reconnection, consistent with the predictions of earlier Hall MHD models,[17–20] and verified by experiment.[21] However, for systems of larger size, the transition to fast reconnection appears to occur at values of Lundquist number that are significantly smaller than the Hall MHD prediction[17–20] due to the intervention of the plasmoid instability.

IV. SUMMARY

In summary, we have demonstrated that within the framework of the resistive MHD model, thin current sheets in systems of large size that exceed a critical value of the Lundquist number are unstable to a super-Alfvénic tearing instability, referred to here as the plasmoid instability. If the aspect ratio of the current sheet is written $\varepsilon \sim S_L^{-\alpha}$, where $\alpha > 0$, the fastest growing instability is characterized by a wave number $\kappa_{\max} \sim S_L^{(5\alpha-1)/4}$ and a growth rate $\gamma_{L,\max} \sim S_L^{(3\alpha-1)/2}$. In the special case of a Sweet–Parker current sheet for which $\alpha = 1/2$, we obtain the instability discussed in Ref. 11. As a result of this class of instabilities, the system realizes a nonlinear reconnection rate that appears to be weakly dependent on the Lundquist number, and larger than the Sweet–Parker rate by an order of magnitude (for the range of Lundquist numbers considered in the present study). We note that this weak dependency on the Lundquist number is realized in a thin current sheet that is violently unstable and dynamic, but not turbulent. In this respect, our results are different from those obtained from turbulent reconnection studies in two [10,22,23] as well as three dimensions,[24,25] which also report reconnection rates that depend weakly on the resistivity.

ACKNOWLEDGMENTS

This research is supported by the Department of Energy under Grant No. DE-FG02-07ER46372, by NASA under Grant Nos. NNX06AC19G and NNX09AJ86G, and by NSF under Grant No. ATM-090315. Supercomputing support is provided by the National Energy Research Supercomputing Center.

[1] P. A. Sweet, Nuovo Cimento Suppl. **8**, 188 (1958).
[2] E. N. Parker, Astrophys. J., Suppl. Ser. **8**, 177 (1963).
[3] H. E. Petschek, in *AAS/NASA Symposium on the Physics of Solar Flares*, edited by W. N. Hess (NASA, Washington, DC, 1964), p. 425.
[4] B. B. Kadomtsev, Fiz. Plazmy **1**, 710 (1975) [Sov. J. Plasma Phys. **2**, 389 (1976)].
[5] S. Bulanov, J. Sakai, and S. Syrovtaskii, Sov. J. Plasma Phys. **5**, 157 (1979).
[6] L. C. Lee and Z. F. Fu, J. Geophys. Res. **91**, 6807, doi:10.1029/JA091iA06p06807 (1986).
[7] D. Biskamp, Phys. Fluids **29**, 1520 (1986).
[8] M. Yan, L. Lee, and E. R. Priest, J. Geophys. Res. **97**, 8277, doi:10.1029/92JA00170 (1992).
[9] K. Shibata and S. Tanuma, Earth, Planets Space **53**, 473 (2001).
[10] G. Lapenta, Phys. Rev. Lett. **100**, 235001 (2008).
[11] N. F. Loureiro, A. A. Schekochihin, and S. C. Cowley, Phys. Plasmas **14**, 100703 (2007).
[12] L. Ni, A. Bhattacharjee, and H. Yang, Bull. Am. Phys. Soc. **53**, 94 (2008).
[13] R. Samtaney, N. F. Loureiro, D. A. Uzdensky, A. Schekochihin, and S. C. Cowley, Phys. Rev. Lett. **103**, 105004 (2009).
[14] B. Coppi, R. Galvao, R. Pellat, M. N. Rosenbluth, and P. Rutherford, Sov. J. Plasma Phys. **2**, 533 (1976).
[15] P. N. Guzdar, J. F. Drake, D. McCarthy, A. B. Hassam, and C. S. Liu, Phys. Fluids B **5**, 3712 (1993).
[16] W. Daughton, V. Roytershteyn, B. J. Albright, H. Karimabadi, L. Yin, and K. J. Bowers, Phys. Rev. Lett. **103**, 065004 (2009).
[17] Z. W. Ma and A. Bhattacharjee, Geophys. Res. Lett. **23**, 1673, doi:10.1029/96GL01600 (1996).
[18] A. Bhattacharjee, Annu. Rev. Astron. Astrophys. **42**, 365 (2004).
[19] P. Cassak, M. Shay, and J. Drake, Phys. Rev. Lett. **95**, 235002 (2005).
[20] A. N. Simakov and L. Chacon, Phys. Rev. Lett. **101**, 105003 (2008).
[21] M. Yamada, Y. Ren, H. Ji, J. Breslau, S. Gerhardt, R. Kulsrud, and A. Kuritsyn, Phys. Plasmas **13**, 052119 (2006).
[22] W. Matthaeus and S. Lamkin, Phys. Fluids **29**, 2513 (1986).
[23] N. F. Loureiro, D. A. Uzdensky, A. A. Schekochihin, S. C. Cowley, and T. A. Yousef, Mon. Not. R. Astron. Soc. **399**, L146 (2009).
[24] A. Lazarian and E. T. Vishniac, Astrophys. J. **517**, 700 (1999).
[25] G. Kowal, A. Lazarian, E. T. Vishniac, and K. Otmianowska-Mazur, Astrophys. J. **700**, 63 (2009).